Feng Hu*, Yan Sun and Maofei Mei

Systematic calculations of energy levels and transitions rates in Mo XXVIII

https://doi.org/10.1515/zna-2020-0119 Received April 30, 2020; accepted June 5, 2020; published online August 7, 2020

Abstract: Complete and consistent atomic data, including excitation energies, lifetimes, wavelengths, hyperfine structures, Landé g_r-factors and E1, E2, M1, and M2 line strengths, oscillator strengths, transitions rates are reported for the low-lying 41 levels of Mo XXVIII, belonging to the n = 3 states $(1s^22s^22p^6)3s^23p^3$, $3s3p^4$, and $3s^23p^23d$. Highaccuracy calculations have been performed as benchmarks in the request for accurate treatments of relativity, electron correlation, and quantum electrodynamic (QED) effects in multi-valence-electron systems. Comparisons are made between the present two data sets, as well as with the experimental results and the experimentally compiled energy values of the National Institute for Standards and Technology wherever available. The calculated values including core-valence correction are found to be in a good agreement with other theoretical and experimental values. The present results are accurate enough for identification and deblending of emission lines involving the n = 3 levels, and are also useful for modeling and diagnosing plasmas.

Keywords: energy levels; lifetimes; transition probabilities; wavelengths.

1 Introduction

The concentration of impurities in the plasma and their radiated power through line emission inside the radius of the limiter or the magnetic separatrix are of great concern for tokamak fusion physics devices [1]. The molybdenum content in the plasma was of great concern because their radiation could cause problems in attaining the highest performing pure plasmas [2]. In laser-produced plasma

light sources used in the soft X-ray and extreme ultraviolet (EUV) spectral regions, targets of various elements are used to produce suitable wavelengths for specific applications [3]. The selection of target element (Mo) is also critical to maximize emission in the water-window soft X-ray spectral region to develop the most efficient sources for biomedical microscopy and cell tomography [4]. The laser-produced Mo plasma have been provided data for opacity, which is crucial to energy transport by radiation in hot-dense plasma, astrophysics, inertial confinement fusion, and other high energy density physics domains [5]. These applications need a large amount of atomic data to describe the different ionization degree of molybdenum. But for P-like Mo, radiative data have only been published from few works.

In the experimental front, few lines of Mo XV-XXXIII were observed from a spark spectrum by Scheob et al. [6]. A number of spectrum lines arising from magnetic dipole transitions in the $3s^{x}3p^{y}$ (x = 1, 2, and y = 1, 2, 3, 4, 5) configurations in elements $29 \le Z \le 42$ have been observed in the Princeton Large Torus (PLT) tokamak discharges by Denne et al. [7]. The energy-level structure of the $3s^23p^3$ configurations of Mo XXVIII were determined from magnetic-dipole line wavelengths and emissivities measured in the PLT by Denne et al. [8]. Relative intensity measurements of various lines pairs resulting from magnetic-dipole transitions within the configurations $3s^23p^3$ were presented by Denne and Hinnov [9]. Transitions of the types $3s^23p^k-3s3p^{k+1}$ and $3p^{k}-3p^{k-1}$ 3d were identified by Finkenthal *et al.* in spectra of Mo from PLT tokamak [10]. Phosphoruslike spectra of Mo XXVIII were obtained with the tokamak plasams in the wavelength range of 83 to 163 Å by Sugar et al. [11]. The classification of 15 new n = 3, $\Delta n = 0$ transitions in Mo XXVIII were made by Jupén et al. [12]. Spectra of Mo were investigated by Chowdhuri et al. with the large helical device plasmas [13].

In the theoretical front, calculations based on a simple shell solution for Mo XXVIII were done by Carlson *et al.* [14]. Scaled Hartree–Fock radial integrals were used by Sugar and Kaufanm in calculating the energy levels of the $3s^23p^3$ configurations of Molybdenum [15]. The multiconfiguration Dirac–Fock technique was used to calculate energy levels of P-like sequences by Huang [16]. The Hartree–Fock–

^{*}Corresponding author: Feng Hu, School of Physics and New Energy, Xuzhou University of Technology, Xuzhou, Jiangsu, 221018, People's Republic of China, E-mail: hufengscu@139.com. https://orcid.org/0000-0003-1453-2326

Yan Sun and Maofei Mei: School of Physics and New Energy, Xuzhou University of Technology, Xuzhou, Jiangsu, 221018, People's Republic of China

Slater method was used to energy levels and wavelengths in Mo XX- Mo XL by Câmpecanu et al. [17].

New computations can match measurement, fill gaps, and suggest revisions closely with almost spectroscopic accuracy, which is a critical assessment of theoretical calculations of structure and transition probabilities from the experimenter's view conducted by Träert [18]. These theoretical citations as well as the ones for experimental data are certainly incomplete. Previous calculations were a number of P-like ions calculations, and the attention was paid to the trend. Limited sets of configurations were discussed [14, 15, 17], or the results were given in the form of diagram [16]. A complete and consistent data set is in demand due to their importance in calculating accurate radiative transition probabilities, which was proved in Al-like Mo calculated by Hu et al. [19]. In some cases, especially when strong self-absorption effects exist, corresponding results for forbidden transitions, such as magnetic dipole (M1), electric quadrupole (E2), and magnetic quadrupole (M2) transitions, are also necessary for modeling and diagnostics of plasmas [1].

In the present work, the multiconfiguration Dirac-Hartree-Fcok method is performed to report energies, E1, M1, E2, and M2 radiative transition properties for Mo XXVIII using the new version of GRASP2018 [20]. Based on our previous work [21, 22], in this paper, the valencevalence (VV) and core-valence (CV) correlation effects are considered in a systematic way. Breit interactions and quantum electrodynamics (QED) effects have been added. This computational approach enables us to present a consistent and improved data set of all important E1, M1, E2, and M2 transitions of the Mo XXVIII spectra, which are useful for identifying transition lines in further investigations.

2 Method

2.1 MCDHF and RCI

The multiconfiguration Dirac-Hartree-Fock (MCDHF) method has recently been described in great detail by Jönsson et al. [23, 24]. Hence we only repeat the essential features here. Starting from the Dirac-Coulomb Hamiltonian

$$H_{DC} = \sum_{i=1}^{N} \left(c\alpha_i \cdot p_i + (\beta_i - 1)c^2 + V_i^N \right) + \sum_{i>j}^{N} \frac{1}{r_{ij}}$$
 (1)

where V^N is the monopole part of the electron-nucleus Coulomb interaction, the atomic state functions (ASFs) describing different finestructure states are obtained as linear combinations of symmetry adapted configuration state functions (CSFs)

$$|\gamma J M_J\rangle = \sum_{j=1}^{N_{CSFs}} c_j |\gamma_j J M_J\rangle \tag{2}$$

In the expression above I and M_I are the angular quantum numbers. y denotes other appropriate labeling of the CSF, for example parity, orbital occupancy, and coupling scheme. The CSFs are built from products of one-electron Dirac orbitals. In the relativistic selfconsistent field (RSCF) procedure both the radial parts of the Dirac orbitals and the expansion coefficients are optimized to selfconsistency. The Breit interaction

$$H_{Breit} = -\sum_{i < j}^{N} \left[\alpha_{i} \cdot \alpha_{j} \frac{\cos(\omega_{ij} r_{ij}/c)}{r_{ij}} + (\alpha_{i} \cdot \nabla_{i}) (\alpha_{j} \cdot \nabla_{j}) \frac{\cos(\omega_{ij} r_{ij}/c) - 1}{\omega_{ij}^{2} r_{ij}/c^{2}} \right]$$
(3)

as well as leading QED corrections can be included in subsequent relativistic configuration interaction (RCI) calculations [25]. Calculations can be done for single levels, but also for portions of a spectrum in the extended optimal level (EOL) scheme, where optimization is on a weighted sum of energies [26]. Using the latter scheme a balanced description of a number of fine-structure states belonging to one or more configurations can be obtained in a single calculation.

2.2 Calculation procedure

The $(1s^22s^22p^6)3s^23p^3$, $3s3p^4$, and $3s^23p^23d$ configurations define the multireference (MR) for the even and odd parities, respectively. As a starting point MCDHF calculations in the EOL scheme were performed for even and odd states using configuration expansions including all lower states of the same *J* symmetry and parity, and a Dirac–Coulomb version was used, for the optimization of the orbitals, including Breit corrections in a final configuration interaction calculation [27]. The calculations for the even states and odd states were based on CSF expansions obtained respectively by allowing single (S) and double (D) substitutions of orbitals in the even and odd MR configurations to an increasing active set (AS) of orbitals. More configurations sets can result in a considerable increase of computational time required for the problem, and appropriate restrictions may be necessary. Even states and odd states are optimized a set of increasing orbitals independently.

In order to consider the correlation effects, the Valence-Valence and Core-Valence calculations were considered in a systematic way. The similar calculation produce have been introduced in ref [21]. For P-like ions, $3s^23p^3$ and $3s^23p^23d$ configurations are treated as the starting point, where the $3s^23p^3$ configuration with total angular momenta J = 1/2, 3/2 and 5/2, and the $3s^23p^23d$ configuration with total angular momenta I = 1/2, 3/2, 5/2, 7/2 and 9/2.

In the first step, the AS is

$$AS1 = \{3s, 3p, 3d\}$$
 (4)

and then increase the principal number n

$$AS2 = AS1 + \{4s, 4p, 4d, 4f\}$$
 (5)

$$AS3 = AS2 + \{5s, 5p, 5d, 5f, 5g\}$$
 (6)

$$AS4 = AS3 + \{6s, 6p, 6d, 6f, 6g\}$$
 (7)

$$AS5 = AS4 + \{7s, 7p, 7d, 7f, 7g\}$$
 (8)

The VV, and CV used different active set. In VV method, 1s²2s²2p⁶ was set as core electrons in the calculation, 1s²2s²2p⁵ and 1s²2s¹2p⁶ were set as core elections in CV model [21]. The total number of CSFs for VV is 13,4335, while 110,7162 for CV.

3 Results and discussion

The energies for the low-lying 41 levels of $3s^23p^3$, $3s3p^4$, and $3s^23p^23d$ configurations of Mo XXVIII were listed in Table 1. Also listed in this Table 1 are the experimentally complied values of the National Institute of Standards and Technology (NIST) [28]. The NIST database listed the energies for the nine out of the present 41 excited levels in Mo XXVIII. The principal number in this calculation was set to $n \le 7$. There are two reasons for this. One is the convergence as mentioned above. For VV calculation, it is not very difficult to get convergence for higher principal number (n8), but for CV calculation the convergence is difficult. The number of CSFs would increase very rapidly when we include the $n \ge 8$ orbitals, and it is hard to get convergence. Also, because of the computer calculation limit and the problem of the program GRASP2K code itself, we only compare the VV and CV models on an equal footing $(n \le 7)$, as mentioned above. The other is the contribution from n = 7 less than 0.001%. Figure 1 shows the mean (with the standard deviation) of the relative differences between VVn and NIST is -166 and 5645 cm⁻¹. The smallest difference is 990 cm⁻¹ lower than NIST $(3s^2 3p^3 ({}_{3}^2D)^{-2}D_{3/2}^0)$, and the biggest difference can be up to 9270 cm⁻¹ $(3s^2 3p^2 {3p \choose 2}P)^{-3}P 3d^2F_{5/2}$). Figure 2 shows the mean (with the standard deviation) of the relative differences between CVn and NIST is 53 and 1625 cm⁻¹. This can be treated as a good example of calculations with the necessary correlations included. As can be seen from Figure 1 and Figure 2, some results considering more configurations are not better than those with fewer configurations. This can be due to configuration mixing, which will be discussed later.

The corrections due to Breit interaction and QED to the excited levels of Mo XXVIII are shown in Figure 3. Selfenergy and vacuum polarization are the two major components in the QED correction [29]. As can be seen, the contribution of Breit interaction is about 1.12 ~ 1.83% for $3s^23p^3$ and $0.09 \sim 0.86\%$ for $3s3p^4$ and $3s^23p^23d$ levels, and the contribution of QED is $-0.47 \sim -0.19\%$ for $3s^23p^3$ and $-0.25 \sim 0.02\%$ for $3s3p^4$ and $3s^23p^23d$ levels. The excited energy levels of Mo XXVIII are all reduced by the mean value 0.57% due to the inclusion of the Breit interaction and QED corrections. Normal mass shift (NMS) and specific mass shift (SMS) are also included in this calculation. The contribution

of NMS for $3s^23p^3$ is about -0.001%, while -0.0001%for $3s3p^4$ and $3s^23p^23d$ levels. The contribution of SMS for $3s^23p^3$ is about 0.002% and -0.001% $3s3p^4$ and $3s^23p^23d$ levels. So, the contribution of NMS and SMS was not plotted in Figure 3.

The data from VV and CV calculations are compared with the energies from qusairelativistic Hartree-Fock plus configuration interactions given by Applicable Data of Manyelectron Atom energies and Transitions (ADAMANT) [30] in Figure 4. The present results in Figure 4 are VV and CV calculations with n = 7. For $3s^23p^3$, the VV results agree well with NIST in the range of -0.42 to 0.21%, while CV in the range of -0.31 to 0.29%. For $3s^23p^23d$, the VV results agree well with NIST in the range of 0.33 to 0.55%, while CV in the range of 0.04 to 0.28%. The results from ADAMANT are in general agreement with NIST. The difference of $3s^2 3p^2 \binom{3}{2}P$) $^3P 3d$ $^2F_{5/2}$ between NIST and theoretical results can up to 0.68%, which was dubious. This is because all the theoretical results were estimated. And the result of NIST corresponds to the $3s^2 3p^2 ({}_{2}^{3}P)^{-3}P 3d^2D_{5/2}$ is 150,8720 cm⁻¹, while theoretical result is about 127,0000 cm⁻¹. The identification of experimental results is very difficult. The previous results from Jupén et al. [12] were not adopted by NIST. For example, the difference between $3s^2 3p^2 \binom{1}{2}D$ $^1D 3d^2D_{3/2}$ and $3s^2 3p^2 \binom{1}{2}D$) $^1D 3d^2D_{5/2}$ is up to about 15,4000 cm⁻¹ [12], while theoretical result is only about 1000 cm⁻¹.

Dirac-Fock wave functions with a minimum number of radial functions are not sufficient to represent the occupied orbitals. Extra configurations have to be added to adequately represent electron correlations. These extra configurations are represented by CSFs and must have the same angular momentum and parity as the occupied orbitals, which cause a problem in identifying the accurate term for each state. For example, the configuration-mixed wave function for the $3s^2 3p^3 \binom{4}{3}S$ | 4 $S_{3/2}^{\circ}$ level is represented as $3s^2 3p^3 {4S \choose 3}$ $4S_{3/2}^\circ = 0.47 3s^2 3p^3 {4S \choose 3}^4 S^\circ + 0.343 s^2 3p^3$ $\binom{2}{1}P^{2}P^{\circ}$ +0.18 3s² 3p³ $\binom{2}{3}D$) ²D°, where 0.47, 0.34 are 0.18 are contributions. The most important contributions to the total wave function of a given level are those from the major configurations. Clearly, the present VV and CV results are in a general agreement. But the order of $3s^2 3p^2 {3P \choose 2} ^3 P 3d^2 P_{1/2}$, $3s^2 3p^2 {3P \choose 2} ^3 P 3d^4 P_{1/2}$, and $3s^{-2}S3p^4\binom{1}{0}S$) $^2S_{1/2}$ levels is different between VV and CV calculations. This is due to more complex system, which it sometimes happens that two or even more level have the same dominating LS term. These three levels get the same quantum labels in present calculations. The GRASP2018 procedure JJ2LSJ [31] was used to transform ASFs from a *ij*-coupled CSF basis [32] into an *LSJ*-coupled CSF basis and select the dominate LS term for the results. With the help of

Table 1: Energies for 41 levels of Mo as function of increasing active sets of orbitals.

Key	Configurations	VVn = 4	VV n = 5	VVn = 6	VV n = 7	CVn = 4	CVn = 5	CVn = 6	CVn = 7	NIST
1	$3s^2 3p^3 ({}_3^4S)^4 S_{3/2}^0$	0	0	0	0	0	0	0	0	0
2	$3s^2 3p^3({}_{3}^2D) {}^{2}D_{3/2}^{0}$	15,6259	15,6258	15,6288	15,6293	15,6396	15,6413	15,6450	15,6458	15,6960
3	$3s^2 3p^3({}_3^2D) {}^2D_{5/2}^{o}$	20,0910	20,0638	20,0626	20,0620	20,1077	20,0759	20,0745	20,0735	20,0710
4	$3s^2 3p^3({}_1^2P) {}^2P_{1/2}^{o'}$	25,8976	25,8621	25,8520	25,8497	25,9282	25,8791	25,8713	25,8679	25,7940
5	$3s^2 3p^3({}_1^2P)^2 P_{3/2}^0$	41,3240	41,3023	41,2982	41,2972	41,3694	41,3415	41,3401	41,3390	41,3440
6	$3s^{-2}S3p^4({}_{2}^{3}P)^4P_{5/2}$	72,3950	72,4268	72,4344	72,4364	72,4598	72,4677	72,4804	72,4853	
7	$3s^{-2}S3p^4(\frac{3}{2}P)^4P_{3/2}$	80,6701	80,6868	80,6911	80,6919	80,6912	80,6847	80,6920	80,6969	
8	$3s^{-2}S3p^4({}_{2}^{3}P)^{-4}P_{1/2}$	83,3007	83,3138	83,3152	83,3156	83,3558	83,3347	83,3401	83,3423	
9	$3s^2 3p^2({}_{2}^{3}P)^{-3}P3d^{-4}F_{3/2}$	88,7662	88,7511	88,7547	88,7553	88,7517	88,7141	88,7160	88,7217	
10	$3s^{-2}S3p^4(\frac{1}{2}D)^2D_{3/2}$	94,6198	94,5988	94,5987	94,5983	94,5949	94,5447	94,5445	94,5478	
11	$3s^2 3p^2({}_{2}^{3}P) {}^{3}P 3d^4F_{5/2}$	95,1840	95,1442	95,1455	95,1455	95,1124	95,0515	95,0488	95,0551	
12	$3s^{-2}S3p^4({}_2^1D)^2D_{5/2}$	97,5603	97,5502	97,5513	97,5512	97,5777	97,5381	97,5426	97,5470	
13	$3s^2 3p^2({}_{2}^{3}P) {}^{3}P 3d^2P_{3/2}$	100,3832	100,3782	100,3822	100,3828	100,3401	100,3168	100,3212	100,3285	
14	$3s^2 3p^2({}_2^3P) {}^3P 3d {}^2P_{1/2}$	101,3566	101,3473	101,3489	101,3490	101,2997	101,2660	101,2676	101,2737	
15	$3s^2 3p^2({}_2^1D) {}^1D 3d^2F_{5/2}$	103,1119	103,0691	103,0718	103,0721	103,0404	102,9800	102,9785	102,9855	
16	$3s^2 3p^2({}_{2}^{3}P) {}^{3}P 3d^4F_{7/2}$	105,8082	105,7625	105,7659	105,7662	105,7428	105,6765	105,6760	105,6835	
17	$3s^2 3p^2({}_{2}^{3}P) {}^{3}P 3d^4D_{7/2}$	107,1977	107,1589	107,1625	107,1629	107,1344	107,0770	107,0790	107,0874	
18	$3s^2 3p^2 {3 \choose 2} P) ^3 P 3d^4 D_{1/2}$	108,3614	108,3324	108,3302	108,3295	108,2773	108,2153	108,2114	108,2145	
19	$3s^2 3p^2({}_2^3P) {}^3P 3d^4D_{3/2}$	110,1603	110,1341	110,1368	110,1371	110,0590	110,0083	110,0096	110,0158	
20	$3s^2 3p^2({}_{2}^{3}P) {}^{3}P 3d^4F_{9/2}$	111,0241	110,9560	110,9574	110,9571	110,9693	110,8815	110,8785	110,8857	
21	$3s^2 3p^2 {3 \choose 2} P) ^3 P 3d^4 D_{5/2}$	112,9457	112,8934	112,8963	112,8968	112,8111	112,7417	112,7392	112,7459	
22	$3s^{-2}S3p^4({}_2^3P)^2P_{3/2}$	119,2855	119,1560	119,1515	119,1496	119,1227	118,9863	118,9623	118,9616	
23	$3s^2 3p^2({}_2^1D) {}^1D 3d^2G_{7/2}$	119,5529	119,4330	119,4241	119,4224	119,1933	119,0360	119,0218	119,0254	
24	$3s^2 3p^2 {3 \choose 2} P) ^3 P 3d^4 P_{5/2}$	119,9553	119,8416	119,8395	119,8393	119,5924	119,4660	119,4473	119,4502	119,3940
25	$3s^2 3p^2({}_{2}^{3}P) {}^{3}P3d {}^{4}P_{1/2}$	120,4572	120,4147	120,4129	120,4125	120,3063	120,2424	120,2359	120,2399	
26	$3s^2 3p^2({}_2^1D) {}^1D 3d^2P_{3/2}$	122,6531	122,5268	122,5194	122,5176	122,2706	122,1233	122,0949	122,0926	
27	$3s^{-2}S3p^4({}_0^1S)^2S_{1/2}$	122,9293	122,7974	122,7889	122,7866	122,6848	122,5335	122,5044	122,5027	
28	$3s^2 3p^2({}_2^3P) {}^3P 3d^4P_{3/2}$	125,6339	125,4535	125,4358	125,4313	125,4761	125,2751	125,2361	125,2333	
29	$3s^2 3p^2 {3 \choose 2} P) ^3 P 3d^2 D_{5/2}$	127,6041	127,5575	127,5607	127,5610	127,5600	127,3505	127,3090	127,3058	
30	$3s^2 3p^2({}_2^1D) {}^1D 3d^2F_{7/2}$	127,9560	127,7446	127,7315	127,7281	127,5779	127,4977	127,4998	127,5081	
31	$3s^2 3p^2({}_2^1D) {}^1D 3d^2G_{9/2}$	130,1294	130,0250	130,0230	130,0216	130,0958	129,9689	129,9617	129,9673	
32	$3s^{-2}S3p^4({}_2^3P)^{-2}P_{1/2}$	133,2929	133,0894	133,0724	133,0677	132,9474	132,7206	132,6788	132,6741	
33	$3s^2 3p^2({}_2^1D)^1D 3d^2P_{1/2}$	135,0716	134,9677	134,9620	134,9605	134,7162	134,5907	134,5699	134,5702	
34	$3s^2 3p^2({}_2^1D) {}^1D 3d {}^2D_{3/2}$	136,9987	136,8529	136,8459	136,8444	136,6041	136,4382	136,4117	136,4111	
35	$3s^2 3p^2({}_2^1D) {}^1D 3d {}^2D_{5/2}$	137,1112	136,9577	136,9508	136,9495	136,7262	136,5575	136,5308	136,5306	136,4420
36	$3s^2 3p^2({}_2^3P) {}^3P3d {}^2F_{7/2}$	140,8177	140,5888	140,5794	140,5769	140,4550	140,2130	140,1785	140,1778	140,1070
37	$3s^2 3p^2({}_0^1S) {}^1S 3d {}^2D_{5/2}$	141,8296	141,6537	141,6344	141,6287	141,7940	141,5866	141,5531	141,5515	
38	$3s^2 3p^2 \binom{1}{0}S$ $^1S 3d$ $^2D_{3/2}$	144,7637	144,5618	144,5457	144,5415	144,4364	144,2125	144,1694	144,1649	
39	$3s^2 3p^2({}_2^1D)^1D 3d^2S_{1/2}$	149,0069	148,8286	148,8135	148,8099	148,5988	148,4006	148,3673	148,3629	
40	$3s^2 3p^2({}_{2}^{3}P) {}^{3}P 3d^2D_{3/2}$	150,3495	150,1340	150,1173	150,1127	150,0398	149,8002	149,7564	149,7523	
41	$3s^2 3p^2 {3 \choose 2} P)^{-3} P 3d^{-2} F_{5/2}$	151,9508	151,7256	151,7110	151,7075	151,5804	151,3412	151,3002	151,2973	150,8720

JJ2LSJ, the levels $3s^{-2}S3p^4({}_2^3P)^{-2}P_{3/2}$, $3s^23p^2({}_2^1D)^{-1}D3d$ $^{2}G_{7/2}$, 3s $^{2}S3p^{4}(_{2}^{3}P)$ $^{2}P_{1/2}$, and 3s $^{2}3p^{2}(_{2}^{1}D)$ $^{1}D3d$ $^{2}P_{1/2}$ have been adjusted in this calculation. In the present calculations, the nuclear parameters I, μ_I , and Q are all set to 1. The A_I and B_I values for a specific isotope can be scaled with the tabulated values given from Table 2.

Among the calculated wavelengths of transition between the lowest 41 levels in Mo XXVIII, the experimental data compiled by NIST listed the observed wavelengths for four E1 transitions and six M1 transitions. The observed results are from Denne et al. [8] and Sugar

et al. [11]. Also, the wavelengths from Jupén et al. [12], which were not compiled by NIST. The accuracy of calculated CV and VV wavelengths relative to experimental results can be assessed from Table 3, where the agreement is within 0.07 Å for CV calculation except the transition $3s^2S 3p^4 \binom{3}{2}P$) $^4P_{3/2} - 3s^2 3p^3 \binom{4}{3}S$) $^4S_{3/2}^o$ with a calculated wavelength $\lambda = 84.771 \text{ Å}$ deviates from the measure by about 0.21 Å. The difference between VV and observed results is in the range of $-0.09 \sim -0.49$ Å. The wavelength of $3s^2 3p^2 {3p \choose 2} P$ $^3 P 3d ^4 P_{3/2} - 3s^2 3p^3 {2p \choose 1} ^2 P_{3/2}^0$ (not listed in Table 3) adopted by NIST is 91.301 Å, which

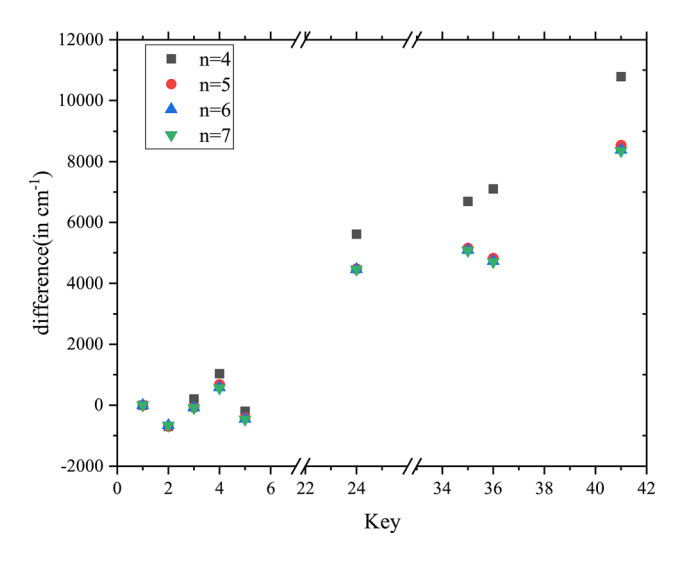


Figure 1: Energy difference between the valence-valence correlation results and the energies for the nine out of the lowest 41 levels from NIST.

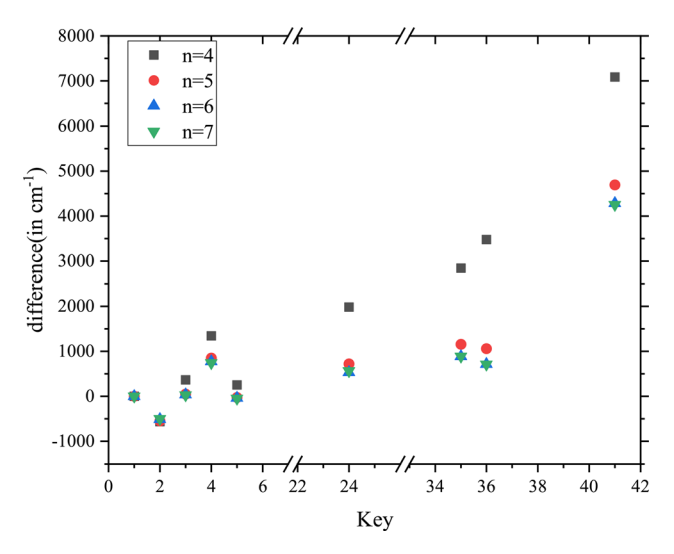


Figure 2: Energy difference between the Core-valence correlation results and the energies for the nine out of the lowest 41 levels from NIST.

corresponding to the transition $3s^2 3p^2 \left(\frac{3}{2}P\right)^{-3}P3d^{-4}P_{3/2}-3s^2 3p^3 \left(\frac{3}{1}P\right)^{-2}P_{3/2}^o$ in CV and VV calculation. The differences between CV and experimental results are in the range of $-0.012 \sim -0.213$ Å for E1 transitions and $-0.58 \sim 2.96$ Å for M2 transitions. The VV results are in the range of $-0.098 \sim -0.493$ Å for E1 and $-1.27 \sim -2.94$ Å for M2. The result of M2 transition $3s^2 3p^3 \left(\frac{3}{3}D\right)^{-2}D_{3/2}^o - 3s^2 3p^3 \left(\frac{4}{3}S\right)^{-4}S_{3/2}^o$ is overestimated about 26 Å.

Lifetime is a measurable datum, and it can be a good check on the accuracy of present calculation [22]. Lifetimes for the lower 36 levels in Mo XXVIII in length and velocity

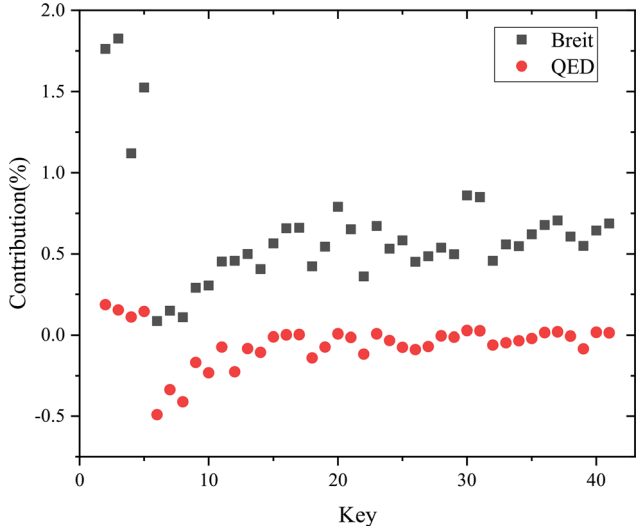


Figure 3: The effect of the Breit interaction and QED corrections on the excitation energies of the Mo XXVIII configurations obtained from the present MCDHF calculations.

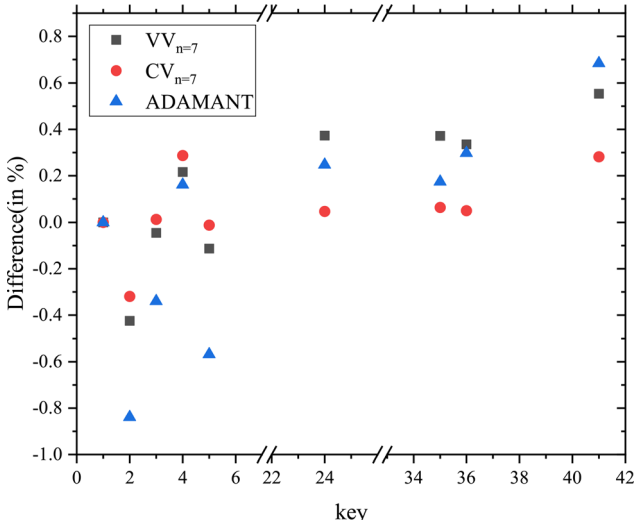


Figure 4: Difference (in %) of various theoretical energies from the NIST complied values in Mo XXVIII.

are listed in Table 4. Contributions from all possible E1 and M2 radiative decays are included in lifetimes, and dominated by E1 transitions. The value τ_l/τ_v for CV calculations is in range of 0.923 ~ 1.093, while 0.960 ~ 1.196 for VV calculations. To assess the accuracy of these theoretical results, the ratios of CV_{τ_l}/VV_{τ_l} and VV_{τ_v}/VV_{τ_v} are also listed in Table 4. The mean ratio of CV_{τ_l}/VV_{τ_l} is 1.021 and 1.051 for VV_{τ_v}/VV_{τ_v} . Lifetimes of $3s^2 3p^2(\frac{3}{2}P)^{-3}P3d^{-4}F_{9/2}$ and $3s^2 3p^2(\frac{1}{2}D)^{-1}D3d^{-2}G_{9/2}$ are 0.176 and 1.389 ms, which are very stable and can be measured in the future.

Table 2: LS-composition, A_i , B_i hyperfine interaction constants, and Landé g_{Γ} factors for the lowest 41 levels in Mo XXVIII.

Key		A(MHz)	B(MHz)	g ,		
	CV	vv				
1	0.47(1) + 0.34(5) + 0.18(2)	0.47(1) + 0.34(4) + 0.18(2)	2.315(4)	3.412(4)	1.551	
2	0.52(2) + 0.40(1) + 0.05(5)	0.52(2) + 0.40(1) + 0.05(5)	7.701(3)	2.442(4)	1.319	
3	0.98(3)	0.98(3)	5.546(4)	-1.237(2)	1.196	
4	0.97(4)	0.97(4)	1.603(5)	0.000(0)	0.662	
5	0.59(5) + 0.28(2) + 0.11(1)	0.59(5) + 0.28(2) + 0.11(1)	3.068(4)	-5.867(4)	1.252	
6	0.76(6) + 0.12(12) + 0.08(24)	0.76(6) + 0.12(12) + 0.08(24)	1.141(5)	2.644(4)	1.537	
7	0.39(7) + 0.18(10) + 0.10(22)	0.40(7) + 0.17(10) + 0.09(22)	3.992(3)	-3.379(4)	1.325	
8	0.60(8) + 0.26(27) + 0.09(25)	0.60(8) + 0.25(27) + 0.09(25)	3.515(5)	0.000(0)	2.451	
9	0.34(9) + 0.33(7) + 0.11(38)	0.33(9) + 0.33(7) + 0.11(38)	5.725(4)	-7.650(3)	1.061	
10	0.38(10) + 0.18(9) + 0.11(7)	0.38(10) + 0.18(9) + 0.11(7)	7.579(3)	-2.580(4)	0.927	
11	0.40(11) + 0.17(21) + 0.14(37)	0.40(11) + 0.17(21) + 0.14(37)	3.345(4)	-6.544(3)	1.162	
12	0.51(12) + 0.18(35) + 0.14(21)	0.50(12) + 0.18(35) + 0.14(21)	9.715(4)	-4.349(4)	1.242	
13	0.34(13) + 0.19(9) + 0.12(22)	0.34(13) + 0.19(9) + 0.12(22)	3.001(4)	-1.838(4)	1.062	
14	0.24(14) + 0.38(18) + 0.16(32)	0.08(27) + 0.38(18) + 0.25(14)	4.946(4)	0.000(0)	7.077	
15	0.36(15) + 0.32(11) + 0.24(41)	0.36(15) + 0.32(11) + 0.25(41)	4.456(4)	-1.906(4)	0.937	
16	0.70(16) + 0.16(23) + 0.09(30)	0.70(16) + 0.16(23) + 0.09(30)	2.832(4)	1.263(4)	1.168	
17	0.48(17) + 0.24(30) + 0.15(36)	0.48(17) + 0.24(30) + 0.15(36)	8.700(3)	5.418(4)	1.275	
18	0.49(18) + 0.16(27) + 0.15(32)	0.49(18) + 0.16(27) + 0.15(32)	7.115(4)	0.000(0)	0.823	
19	0.54(19) + 0.11(32) + 0.10(10)	0.55(19) + 0.11(32) + 0.10(10)	2.662(3)	-2.331(4)	1.132	
20	0.63(20) + 0.36(31)	0.63(20) + 0.36(31)	2.832(4)	1.389(4)	1.249	
21	0.32(21) + 0.17(11) + 0.15(24)	0.33(21) + 0.17(11) + 0.14(24)	2.831(4)	-2.164(4)	1.209	
22	0.32(22) + 0.15(13) + 0.12(34)	0.59(23) + 0.14(16) + 0.13(17)	3.295(4)	4.602(4)	1.039	
23	0.58(23) + 0.14(16) + 0.12(17)	0.32(22) + 0.14(13) + 0.11(34)	-1.024(4)	1.397(4)	1.179	
24	0.47(24) + 0.20(21) + 0.12(35)	0.48(24) + 0.19(21) + 0.12(35)	2.336(4)	2.147(3)	1.421	
25	0.29(25) + 0.27(14) + 0.25(27)	0.30(14) + 0.26(25) + 0.25(14)	1.532(5)	0.000(0)	1.518	
26	0.34(26) + 0.34(28) + 0.18(32)	0.34(26) + 0.33(28) + 0.18(33)	4.058(4)	-9.008(3)	1.489	
27	0.05(27) + 0.24(39) + 0.21(25)	0.24(25) + 0.24(39) + 0.16(8)	1.696(5)	0.000(0)	1.860	
28	0.08(28) + 0.38(40) + 0.17(38)	0.09(28) + 0.37(40) + 0.17(38)	3.555(4)	1.926(4)	0.911	
29	0.42(29) + 0.19(41) + 0.17(15)	0.36(30) + 0.36(17) + 0.12(36)	1.684(4)	1.729(4)	1.223	
30	0.37(30) + 0.36(17) + 0.12(36)	0.42(29) + 0.19(41) + 0.16(15)	8.368(3)	3.813(4)	1.085	
31	0.63(31) + 0.36(20)	0.63(31) + 0.35(20)	1.911(4)	6.212(4)	1.188	
32	0.21(32) + 0.36(33) + 0.27(39)	0.39(33) + 0.26(39) + 0.19(32)	-2.788(4)	0.000(0)	1.034	
33	0.39(33) + 0.23(25) + 0.20(32)	0.22(32) + 0.35(33) + 0.24(39)	1.367(4)	0.000(0)	1.188	
34	0.43(34) + 0.18(28) + 0.13(10)	0.43(34) + 0.18(28) + 0.13(10)	1.856(4)	-1.792(4)	1.080	
35	0.26(35) + 0.16(15) + 0.15(24)	0.25(35) + 0.16(15) + 0.15(24)	4.078(4)	-2.364(4)	1.177	
36	0.61(36) + 0.23(30) + 0.10(23)	0.61(36) + 0.24(30) + 0.10(23)	2.543(4)	-2.341(3)	1.119	
37	0.51(37) + 0.19(35) + 0.15(38)	0.50(37) + 0.20(34) + 0.15(38)	1.065(4)	7.044(4)	1.203	
38	0.28(38) + 0.29(26) + 0.20(13)	0.28(38) + 0.29(26) + 0.20(13)	1.549(4)	-3.229(3)	1.129	
39	0.34(39) + 0.17(27) + 0.16(32)	0.34(39) + 0.17(27) + 0.16(32)	2.010(5)	0.000(0)	1.723	
40	0.45(40) + 0.27(38) + 0.11(26)	0.46(40) + 0.27(38) + 0.11(26)	1.463(4)	1.391(4)	0.934	
41	0.20(41) + 0.32(29) + 0.17(37)	0.20(41) + 0.32(29) + 0.17(37)	1.808(4)	-3.795(4)	1.105	

The transition rate, the weighted oscillator strength and the line strength were given in Coulomb (velocity) and Babushkin (length) gauges in this calculation. Also, for the electric transitions the relative difference (dT) $(dT = abs(A_l - A_v)/max(A_l/A_v))$ between the transition rates in length and velocity gauges are given. A value close to dT = 0 for an allowed transition is a known accuracy indicator [33]. In many cases the values are reasonably close to zero, see Figure 5. But in other cases, for

example, the difference of transition 3s ${}^2S 3p^4 ({}^1_2D)$ ${}^2D_{3/2}$ $3s^2 3p^3 \binom{2}{1}P$) $^2P_{3/2}^0$ can be larger than 0.455. In particular, these calculations presented provide comprehensive new data for E2, M1, and M2 transitions for Mo XXVIII, which no existent data for public. This will help with the identification of spectral lines of Mo XXVIII. Owing the space limitations, full tables of E1, E2, M1, and M2 transitions data will be provided as the supplemental material in conjunction with the E-mail.

Table 3: Calculated lifetimes (in s) of the lower 36 excited levels in Mo XXVIII. $a(b) = a \times 10^{\circ}$.

Upper	Lower	Туре	Exp	cv	vv
$3s^2 3p^2({}_2^1D) {}^1D 3d {}^2D_{5/2}$	$3s^2 3p^3({}^2_3D) {}^2D^o_{3/2}$	E1	82.773°	82.761	82.464
$3s^2 3p^2(\frac{1}{2}D) ^1D 3d ^2D_{3/2}$	$3s^2 3p^3({}^2_3D) {}^2D^o_{3/2}$	E1	82.955°	82.857	82.857
$3s^2 3p^2 (\frac{3}{2}P)^3 P 3d^{-2}F_{7/2}$	$3s^2 3p^3({}^2_3D) {}^2D^{o}_{5/2}$	E1	83.308 ^b	83.267	82.983
$3s^2 3p^2 (\frac{3}{2}P)$ $^3P 3d$ $^4P_{5/2}$	$3s^2 3p^3({}^4S) {}^4S_{3/2}^0$	E1	83.756 ^b	83.743	83.471
$3s^{-2}S3p^4({}_{2}^{3}P)^{-4}P_{3/2}$	$3s^2 3p^3({}^4S) {}^4S^{0}_{3/2}$	E1	84.229ª	84.157	83.832
$3s^2 3p^2 \binom{1}{0}S$ $^1S 3d^{-2}D_{3/2}$	$3s^2 3p^3({}_1^2P) {}^2P_{1/2}^o$	E1	84.771 ^a	84.558	84.278
$3s^2 3p^2({}_{2}^{1}D) {}^{1}D 3d {}^{2}D_{5/2}$	$3s^2 3p^3({}^2_3D) {}^2D^{0}_{5/2}$	E1	85.932 ^b	85.910	85.594
$3s^2 3p^3({}_3^4S) {}_4S_{3/2}^o$	$3s^2 3p^3({}_1^2P) {}^2P_{1/2}^{o}$	M1	387.69°	386.38	386.42
$3s^2 3p^3({}_3^2D)^{-2}D_{3/2}^{o}$	$3s^2 3p^3({}_1^2P) {}^2P_{3/2}^{o}$	M1	389.89°	389.10	389.13
$3s^2 3p^3({}_{3}^2D) {}^2D_{5/2}^o$	$3s^2 3p^3({}_1^2P) {}^2P_{3/2}^{o}$	M1	470.10°	470.26	470.28
$3s^2 3p^3 ({}_{3}^4S)^4 S_{3/2}^o$	$3s^2 3p^3({}^2_3D) {}^2D^o_{5/2}$	M1	498.23°	497.65	497.67
$3s^2 3p^3({}_3^4S) {}_4S_{3/2}^{0}$	$3s^2 3p^3({}^2_3D) {}^2D^{o}_{3/2}$	M1	637.10°	638.61	638.61
$3s^2 3p^3({}_{1}^{2}P) {}^{2}P_{1/2}^{5/2}$	$3s^2 3p^3({}^{2}P) {}^{2}P_{3/2}^{o'}$	M1	643.10°	646.06	646.04
$3s^2 3p^3({}_3^2D)^2D_{3/2}^{0}$	$3s^2 3p^3({}_3^2D)^{-2}D_{5/2}^o$	M1	2228.54°	2254.56	2255.03

^a from Jupén *et al*. [12].

Table 4: Calculated lifetimes (in s) of the lower 36 excited levels in Mo XXVIII. $a(b) = a \times 10^{b}$.

Key	τ (in s)							Ratio
	CV_t	CV_{v}	VV _l	VV_{ν}	$\overline{\text{CV}_l/\text{CV}_v}$	VV_l/VV_{ν}	CV_l/VV_l	CV_{ν}/VV_{ν}
6	1.474(-10)	1.350(-10)	1.466(-10)	1.464(-10)	1.093	1.001	1.006	0.922
7	7.866(-11)	7.424(-11)	7.845(-11)	7.949(-11)	1.060	0.987	1.003	0.934
8	5.643(-11)	5.320(-11)	5.620(-11)	5.565(-11)	1.061	1.010	1.004	0.956
9	1.439(-10)	1.380(-10)	1.475(-10)	1.448(-10)	1.043	1.019	0.975	0.953
10	4.005(-11)	3.833(-11)	3.998(-11)	3.959(-11)	1.045	1.010	1.002	0.968
11	7.254(-11)	7.399(-11)	7.360(-11)	7.151(-11)	0.980	1.029	0.986	1.035
12	8.798(-11)	8.403(-11)	8.656(-11)	8.768(-11)	1.047	0.987	1.016	0.958
13	1.535(-10)	1.418(-10)	1.515(-10)	1.502(-10)	1.082	1.008	1.014	0.945
14	5.645(-11)	5.313(-11)	5.586(-11)	5.386(-11)	1.063	1.037	1.011	0.986
15	4.514(-10)	4.471(-10)	4.587(-10)	4.442(-10)	1.010	1.033	0.984	1.007
16	2.285(-9)	2.476(-9)	2.281(-9)	2.240(-9)	0.923	1.018	1.002	1.105
17	9.223(-8)	9.973(-8)	8.440(-8)	7.056(-8)	0.925	1.196	1.093	1.413
18	2.328(-11)	2.246(-11)	2.323(-11)	2.249(-11)	1.037	1.033	1.002	0.998
19	2.775(-11)	2.746(-11)	2.822(-11)	2.769(-11)	1.011	1.019	0.983	0.992
20	1.758(-3)	1.758(-3)	1.746(-3)	1.746(-3)	1.000	1.000	1.006	1.006
21	2.171(-11)	2.206(-11)	2.227(-11)	2.145(-11)	0.984	1.038	0.975	1.029
22	3.749(-12)	3.750(-12)	3.653(-12)	3.564(-12)	1.000	1.023	1.027	1.052
23	4.711(-11)	4.959(-11)	4.766(-11)	4.658(-11)	0.950	1.025	0.986	1.065
24	4.888(-12)	4.975(-12)	4.685(-12)	4.531(-12)	0.983	1.034	1.043	1.098
25	9.325(-12)	9.410(-12)	1.061(-11)	1.028(-11)	0.991	1.032	0.879	0.915
26	4.971(-12)	4.952(-12)	4.836(-12)	4.633(-12)	1.004	1.044	1.028	1.069
27	6.162(-12)	6.170(-12)	5.455(-12)	5.226(-12)	0.999	1.044	1.130	1.181
28	1.504(-11)	1.527(-11)	1.377(-11)	1.337(-11)	0.985	1.030	1.092	1.142
29	4.708(-12)	4.825(-12)	3.367(-10)	3.210(-10)	0.976	1.049	1.031	1.094
30	3.310(-10)	3.423(-10)	4.565(-12)	4.410(-12)	0.967	1.035	0.983	1.067
31	1.389(-2)	1.389(-2)	1.397(-2)	1.397(-2)	1.000	1.000	0.994	0.994
32	5.301(-12)	5.331(-12)	5.291(-12)	5.146(-12)	0.994	1.028	1.002	1.036
33	4.453(-12)	4.440(-12)	4.157(-12)	4.020(-12)	1.003	1.034	1.071	1.104
34	3.829(-12)	3.872(-12)	3.708(-12)	3.604(-12)	0.989	1.029	1.033	1.074
35	4.074(-12)	4.150(-12)	3.950(-12)	3.837(-12)	0.982	1.030	1.031	1.082
36	4.138(-12)	4.308(-12)	4.004(-12)	3.923(-12)	0.961	1.021	1.033	1.098

^b from Sugar et al. [11].

from Denne et al. [8].

Table 4: (continued)

Key				τ (in s)				
	CV,	CV _v	VV_l	VV _v	CV_l/CV_v	VV_l/VV_v	CV_l/VV_l	CV_{ν}/VV_{ν}
37	1.148(-10)	1.237(-10)	9.751(-11)	1.016(-10)	0.928	0.960	1.177	1.217
38	4.905(-12)	4.972(-12)	4.701(-12)	4.550(-12)	0.987	1.033	1.043	1.093
39	4.021(-12)	4.061(-12)	3.881(-12)	3.813(-12)	0.990	1.018	1.036	1.065
40	5.310(-12)	5.471(-12)	5.142(-12)	4.987(-12)	0.971	1.031	1.033	1.097
41	4.611(-12)	4.788(-12)	4.475(-12)	4.372(-12)	0.963	1.024	1.030	1.095

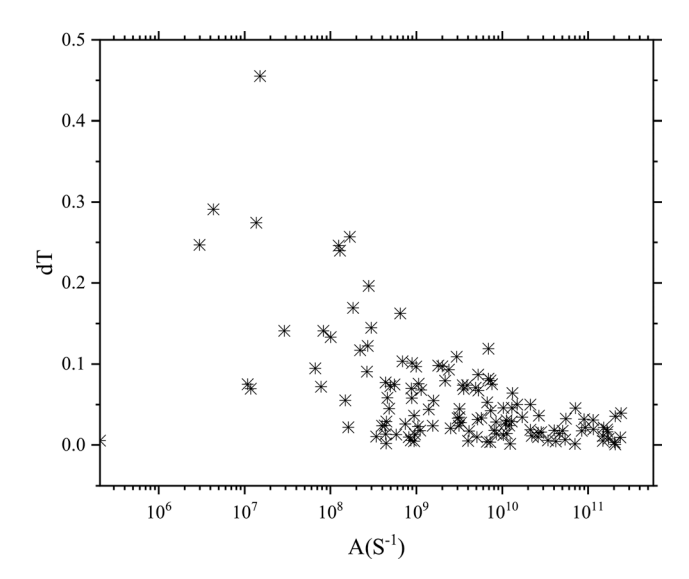


Figure 5: Scatterplot of dT and A (S⁻¹) for all E1 transitions.

4 Conclusions

Using the MCDHF methods with considering the electron correlations, energy levels, lifetimes, wavelengths, hyperfine structures, Landé g_J -factors and E1, E2, M1, and M2 line strengths, oscillator strengths, transitions rates are reported for the low-lying 41 levels belonging to the $3s^23p^3$, $3s3p^4$, and $3s^23p^23d$ configurations of P-like Mo XXVIII have been determined. The accuracy of energy levels and transition probabilities is estimated by comparing VV and CV results with available theoretical and experimental data. Excitation energies are accurate to within 0.04%. The computed wavelengths are almost spectroscopic accuracy, aiding line identification in spectra. Our results are useful for many applications such as controlled thermonuclear fusion, laser and plasma physics as well as astrophysics.

Author contribution: All the authors have accepted responsibility for the entire content of this submitted manuscript and approved submission.

Research funding: None declared.

Conflict of interest statement: The authors declare no conflicts of interest regarding this article.

References

- M. J. May, M. Finkenthal, S. P. Regan, et al., "The measurement of the intrinsic impurities of molybdenum and carbon in the Alcator C-Mod tokamak plasma using low resolution spectroscopy," *Nucl. Fusion*, vol. 37, p. 881, 1997.
- [2] D. M. Meade, "Effect of high-Z impurities on the ignition and Lawson conditions for a thermonuclear reactor," *Nucl. Fusion*, vol. 14, p. 289, 1974.
- [3] T. Tamura, G. Arai, Y. Kondo, et al., "Selection of target elements for laser-produced plasma soft x-ray sources," Opt. Lett., vol. 43, p. 2042, 2018.
- [4] T. Tamura, G. Arai, Y. Kondo, et al., "Soft X-ray emission from molybdenum plasmas generated by dual laser pulses," Appl. Phys. Lett., vol. 109, 2016, Art no. 194103.
- [5] B. Qing, Z. Y. Zhang, M. X. Wei, et al., "Opacity measurements of a molybdenum plasma with open M-shell configurations," *Phys. Plasmas*, vol. 25, 2018, Art no. 023301.
- [6] J. L. Schwob, M. Klapisch, N. Schweitzer, et al., "Identification of Mo XV to Mo XXXIII in the soft X-ray spectrum of the TFR Tokamak," *Phys. Lett. A*, vol. 62, p. 85, 1977.
- [7] B. Denne, E. Hinnov, S. Suckewer, S. Cohen, "Magnetic dipole lines in the 3s²3p* configurations of elements from copper to molybdenum," *Phys. Rev. A*, vol. 28, p. 206, 1983.
- [8] B. Denne, E. Hinnov, S. Suckewer, J. Timberlake, "On the ground configuration of the phosphorus sequence from copper to molybdenum," J. Opt. Soc. Am. B, vol. 1, p. 296, 1984.
- [9] B. Denne, E. Hinnov, "Spectrometer-sensitivity calibration in the extreme ultraviolet by means of branching ratios of magneticdipole lines," J. Opt. Soc. Am. B, vol. 1, p. 699, 1984.
- [10] M. Finkenthal, B. C. Stratton, H. W. Moos, et al., "Spectra of highly ionised zirconium and molybdenum in the 60-150 AA range from PLT tokamak plasmas," J. Phys. B, vol. 18, p. 4393, 1985.
- [11] J. Sugar, V. Kaufman, W. L. Rowan, "Spectra of the Pi isoelectronic sequence from Co XIII to Mo XXVIII," *J. Opt. Soc. Am. B*, vol. 8, p. 22, 1991.
- [12] C. Jupén, B. Denne, E. Hinnov, I. Martinson, L. J. Curtis, "Additions to the Spectra of Highly Ionized Molybdenum, Mo XXIV-Mo XXVIII," *Phys. Scripta*, vol. 68, p. 230, 2003.

- [13] M. B. Chowdhuri, S. Morita, M. Goto, et al., "Line analysis of EUV spectra from molybdenum and tungsten injected with impurity pellets in LHD," Plasma Fusion Res., vol. 2, p. S1060, 2007.
- [14] T. A. Carlson, C. W. Nestor, N. Wasserman, J. D. McDowell, "Calculated ionization potentials for multiply charged ions," Atomic Data Nucl. Data Tables, vol. 2, p. 63, 1970.
- [15] J. Sugar, V. Kaufman, "Predicted wavelengths and transition rates for magnetic-dipole transitions within 3s23pn ground configurations of ionized Cu to Mo," J. Opt. Soc. Am. B, vol. 1, p. 218, 1984.
- [16] K.-N. Huang, "Energy-level scheme and transition probabilities of P-like ions," Atomic Data Nucl. Data Tables, vol. 30, p. 313,
- [17] R. I. Câmpeanu, "HFS energy levels and wavelengths in Mo XX-XL," Rev. Roum. Phys., vol. 30, p. 307, 1985.
- [18] E. Träbert, "Critical assessment of theoretical calculations of atomic structure and transition probabilities: an experimenter's view," Atoms, vol. 2, no. 1, p. 15, 2014.
- [19] F. Hu, Y. Sun, M. F. Mei, "Fine-structure energy levels and radiative rates in Al-like molybdenum," Can. J. Phys., vol. 95, p. 59, 2017.
- [20] C. Froese Fischer, G. Gaigalas, P. Jönsson, J. Bieroń, "GRASP2018 -A Fortran 95 version of the general relativistic atomic structure package," Phys. Commun., vol. 237, p. 184, 2019.
- [21] F. Hu, M. F. Mei, C. Han, et al., "Accurate multiconfiguration Dirac-Hartree-Fock calculations of transition probabilities for magnesium-like ions," J. Quant. Spectrosc. Radiat. Transfer, vol. 149. p. 158. 2014.
- [22] F. Hu, Y. Sun, M. F. Mei, C. C. Sang, J. M. Yang, "Energy levels, radiative rates, and lifetimes for transitions in Fe XIV," J. Appl. Spectrosc., vol. 85, p. 749, 2018.
- [23] P. Jönsson, X. He, C. Froese Fischer, I. P. Grant, "The grasp2K relativistic atomic structure package," Comput. Phys. Commun., vol. 177, no. 7, p. 597, 2007.

- [24] P. Jönsson, G. Gaigalas, J. Bieroń, C. Froese Fischer, I. P. Grant, "New version: Grasp2K relativistic atomic structure package," Comput. Phys. Commun., vol. 184, no. 9, p. 2197, 2013.
- [25] B. J. McKenzie, I. P. Grant, P. H. Norrington, "A program to calculate transverse Breit and QED corrections to energy levels in a multiconfiguration Dirac-Fock environment," Comput. Phys. Commun., vol. 21, no. 2, p. 233, 1980.
- [26] K. G. Dyall, I. P. Grant, C. T. Johnson, F. A. Parpia, E. P. Plummer, "GRASP: A general-purpose relativistic atomic structure program," Comput. Phys. Commun., vol. 55, no. 3, p. 425, 1989.
- [27] I. P. Grant, Relativistic Quantum Theory of Atoms and Molecules, New York, Springer, 2007.
- [28] A. Kramida, Atomic Transition Probability Bibliographic Database, Version 9.0, Gaithersburg, MD, National Institute of Standards and Technology, 2019 [Online]. Available at: https://physics.nist.gov/Elevbib [accessed: Oct. 18, 2019].
- [29] Y. K. Kim, D. H. Baik, P. Indelicato J. P. Desclaux, "Resonance transition energies of Li-, Na-, and Cu-like ions," Phys. Rev. A, vol. 44, p. 148, 1991.
- [30] ADAMANT(Applicable Data of Many-electron Atom energies and Transitions) [Online]. Available at: http://158.129.165.241/ege. php [accessed: Oct. 29, 2019].
- [31] G. Gaigalas, C. Froese Fischer, P. Rynkun, P. Jönsson, "JJ2LSJ transformation and unique labeling for energy levels," Atoms, vol. 5, p. 6, 2017.
- [32] C. Nazé, E. Gaidamauskas, G. Gaigalas, M. Goderfroid, P. Jönsson, Comput. Phys. Commun., vol. 184, p. 2187, 2013.
- [33] J. Ekman, M. R. Godefroid, H. Hartman, "Validation and implementation of uncertainty estimates of calculated transition rates," Atoms, vol. 2, p. 215, 2014.

Supplementary Material: The online version of this article offers supplementary material (https://doi.org/10.1515/zna-2020-0119).